

IMPACTS OF OBSERVATION STRATEGIES ON MICROLENSING TIME DELAYS

KAI LIAO¹

¹ School of Science, Wuhan University of Technology, Wuhan 430070, China

Draft version December 22, 2024

ABSTRACT

Microlensing not only brings extra magnification lightcurves on top of the intrinsic ones but also shifts them in time domain, making the actual time delays between images of strongly lensed AGN change on the \sim day(s) light-crossing time scale of the emission region. The microlensing-induced time delays would bias strong lens time delay cosmography if uncounted. However, due to the uncertainty of the disk size and the disk model, the impact is hard to accurately estimate. In this work, we study how to reduce the bias with designed observation strategy based on a standard disk model. We find long time monitoring of the images could alleviate the impact since it averages the microlensing time lag maps due to the peculiar motion of the source relative to the lens galaxy. In addition, images in bluer bands correspond to smaller disk sizes and therefore benefit time delay measurements as well. We conduct a simulation based on a PG 1115+080-like lensed quasar measured in u and r band, respectively. The campaign is assumed to be 20 years which is the typical limitation for a dedicated program. The results show the time delay dispersions caused by microlensing can be reduced by $\sim 40\%$ with 20-year lightcurves while u band relative to r band reduces $\sim 75\%$ of the dispersions. Nevertheless, such an effect can not be totally eliminated in any cases. Further studies are still needed to appropriately incorporate it in inferring an accurate Hubble constant.

Subject headings: gravitational lensing - accretion disks - quasars: general

1. INTRODUCTION

The issue on the Hubble constant (H_0) is one of the severest concerns for current cosmology since the value inferred from the early-time cosmic microwave background (CMB) observations (Planck Collaboration 2018) is inconsistent with that measured by the late-time distance ladders (Riess et al. 2019). The discrepancy implies either unknown systematic errors or new physics. A third-party approach is expected to bring new perspectives and be the referee.

Strong lensing by galaxies is one of such approaches (Treu & Marshall 2016). A distant quasar is lensed by the foreground elliptical galaxy, forming multiple images of the AGN which arrive at the earth in turn. The time delay between any two of the images is inversely proportional to H_0 and weakly depends on other cosmological parameters as well. With the lens potential information from high-resolution imaging of the host galaxy and spectroscopics, time delay measurements can be used to infer H_0 . The state-of-art lensing program H0LiCOW has achieved a 2.4% precision of H_0 measurement with time delay method (Wong et al. 2020) in agreement of the results from distance ladders. Inspired by the achievement, the new collaboration team TDCOSMO (Millon et al. 2019) will go further to measure H_0 with 1% precision. However, before combining more lenses to get more precise constraint, factors that impact the accuracy of the inference should be addressed, i.e., accuracy is more important than pursuing precision.

Inferring H_0 with time-delay lensing needs at least three ingredients: 1) lens potentials; 2) time delays; 3) mass density fluctuations along the line-of-sight. Challenges on the accuracy of each one are proposed. For example, the lens modelling may bring dom-

inated bias (Schneider & Sluse 2013; Birrer et al. 2016; Ding et al. 2020). For the time delay measurements, the Time Delay Challenge (TDC) program (Liao et al. 2015) proved the bias can be well-controlled, i.e., measurements with lightcurves contaminated by the magnification patterns of microlensing are accurate. However, such a time delay measurement was recently pointed out not to be the cosmologically concerned one (Tie & Kochanek 2018) and it depends on the observing band as well (Liao 2020).

Time delays are measured by comparing the phases of the lightcurve pairs. In fact, gravitational microlensing also produces changes in the actual time delays on the \sim day(s) light-crossing time-scale of the emission region of the accretion disk. This effect is due to a combination of the inclination of the disk relative to the line of sight and the differential magnification of the temperature fluctuations producing the variability (Tie & Kochanek 2018) which changes the arriving timings of the lightcurve phases. Directly verifying such an effect can be done by measuring the time delay difference between bands or time delay ratio anomalies (Liao 2020). For cosmological studies, this effect would bias H_0 inference if uncounted, especially for small time delays. In principle, one can get the microlensing time delay distributions and incorporate them within the Bayesian framework (Chen et al. 2018) (though the time delays at different epochs should be correlated in their analysis). However, the most uncertain factor comes from the disk size (and disk model itself) which has been found to be larger than that predicted by the standard thin-disk model of AGN with reverberation mapping of the continuum emission and microlensing (Collier et al. 1998; Sergeev et al. 2005; Shappee et al. 2014; Fausnaugh et al. 2016;

Jiang et al. 2017; Pooley et al. 2007; Mosquera et al. 2013; MacLeod et al. 2015). It is therefore impossible to correctly understand the prior distributions. The current analysis has not considered such an effect due to not finding time delay variations with observing time (but the effect may still exist) (Bonvin et al. 2018; Wong et al. 2020). Another reason is the H0LiCOW team has chosen the largest time delays such that the relative errors become negligible. However, systems like lens PG 1115+080 which has short time delays would be affected. Ignoring such an effect would limit the lens selection. Note that most works in the literature considered a motionless source which is not realistic. The source would travel along a line in the time lag maps with finite monitoring time due to its peculiar motion relative to the lens galaxy. The microlensing time delay effect is therefore supposed to be averaged.

In this work, rather than discussing how to correctly estimate the impact by microlensing time delays, we study the possibility that increasing the monitoring time in bluer bands can reduce the impact such that the results can be accurate to the greatest extent without considering such an effect. The paper is organized as follows: In Section 2, we introduce the chromatic microlensing time delay effect; In Section 3, we discuss the finite lightcurve case; Simulations and results are presented in Section 4; Finally, we summarize and make discussions in Section 5. To avoid confusion, we use the term “time lag” for single image while “time delay” for that between lensed images.

2. CHROMATIC MICROLENSING TIME DELAYS

Though details of accretion disk models are being debated, a simple thin-disk model is widely concerned as the standard one (Shakura & Sunyaev 1973). For a non-relativistic, thin-disk model that emits as a blackbody, the characteristic size of the disk is defined as

$$R_0 = \left[\frac{45G\lambda_{\text{rest}}^4 M_{\text{BH}} \dot{M}}{16\pi^6 h_p c^2} \right]^{1/3} \\ = 9.7 \times 10^{15} \left(\frac{\lambda_{\text{rest}}}{\mu\text{m}} \right)^{4/3} \left(\frac{M_{\text{BH}}}{10^9 M_\odot} \right)^{2/3} \left(\frac{L}{\eta L_E} \right)^{1/3} \text{ cm}, \quad (1)$$

which corresponds to the radius where the temperature matches the photon rest-frame wavelength, i.e., $kT = h_p c / \lambda_{\text{rest}}$. k, G, h_p, c are Boltzmann, Newtonian, Planck constants and speed of light, respectively. M_{BH} is the mass of the black hole. L/L_E is the fractional luminosity with respect to the Eddington luminosity. $\eta = L/\dot{M}c^2$ is the accretion efficiency ranging from ~ 0.1 to ~ 0.4 that positively correlates with the black hole spin. Note that adjusting to η can not result in the observed larger disk size with current measurement precision. The corresponding characteristic time scale:

$$\frac{(1+z_s)R_0}{c} \simeq \frac{3.8 \text{ days}}{(1+z_s)^{1/3}} \left(\frac{\lambda_{\text{obs}}}{\mu\text{m}} \right)^{4/3} \left(\frac{M_{\text{BH}}}{10^9 M_\odot} \right)^{2/3} \left(\frac{L}{\eta L_E} \right)^{1/3} \quad (2)$$

It is convenient to define a dimensionless radius:

$$\xi = \frac{hc}{kT_0(R)\lambda} = \left(\frac{R}{R_0} \right)^{3/4} \left(1 - \sqrt{\frac{R_{\text{in}}}{R}} \right)^{-1/4}, \quad (3)$$

where R_{in} is the inner edge of the disk (Morgan et al. 2010), depending on whether it is a Schwarzschild or Kerr black hole. The unperturbed temperature profile and surface brightness profile of the disk are given by $T_0(R)^4 \propto R^{-3}(1 - \sqrt{R_{\text{in}}/R})$ and $I_0(R) \propto (e^\xi - 1)^{-1}$, respectively.

For the variability, in a “lamp post” model (Cackett et al. 2007), the fractional temperature variation is independent of the position in the disk. The disk center acts as the driving source, resulting in variability lagged by the light travel time R/c . Assuming the variations are small, the blackbody function can be Taylor expanded and the brightness variability is given by

$$\delta I(R, t) \propto f(t - R/c)G(\xi), \quad (4)$$

where

$$G(\xi) = \frac{\xi e^\xi}{(e^\xi - 1)^2}. \quad (5)$$

Note what one can measure is the phase difference of the light curves between lensed images as the time delay Δt_{lc} . Microlensing makes different parts of the disk contribute differently, inducing different time lags for each image (we refer (Tie & Kochanek 2018) for more details). The mean time lag caused by microlensing is given by (Tie & Kochanek 2018; Liao 2020)

$$t_{\text{micro}} = \frac{1+z_s}{c} \frac{\int dudv G(\xi) M(u, v) R(1 - \cos\theta \sin\beta)}{\int dudv G(\xi) M(u, v)} - t_{\text{disk}}, \quad (6)$$

where $M(u, v)$ is the microlensing magnification map projected in the source plane, θ is the polar angle in the accretion disk plane, β is the inclination angle with $\beta = 0$ corresponding to a face-on disk. $u = R \cos\theta \cos\beta$ and $v = R \sin\theta$ are the coordinates in the source plane. The *geometric delay* appearing in the reverberation mapping method by the disk itself is

$$t_{\text{disk}} = \frac{1+z_s}{c} \frac{\int dudv G(\xi) R(1 - \cos\theta \sin\beta)}{\int dudv G(\xi)}, \quad (7)$$

which corresponds to the case without microlensing. Ignoring the inner edge of the disk, $t_{\text{disk}} = 5.04(1+z_s)R_0/c$. In Eq.6 the integral radius is from R_{in} to infinity. In practice, a $30R_0$ region is sufficient. We set $R_{\text{in}} = R_0/100$ whose specific value impact little. The microlensing time lag primarily depends on the disk size, and weakly depends on the view angles as well (Tie & Kochanek 2018; Bonvin et al. 2018; Liao 2020). The measured time delay relative to the cosmological one is therefore changed by $\Delta t_{\text{lc}} = \Delta t_{\text{cosm}} + \Delta t_{\text{micro}}$.

Moreover, the microlensing time delays was proposed to be chromatic (Liao 2020) since the disk size is a function of wavelength, i.e., time delays measured with lightcurves in different bands are different: $\delta\Delta t_{\text{lc}} \neq 0$. Bluer bands would have smaller effects. Since multiple concepts of time exist, to avoid confusion, we have adopted the sign convention made by (Liao 2020): t without prefix denotes time lag relative to the driving source $f(t)$ for single image, Δ is for difference between images (time delay), δ is for difference between bands and \mathcal{T} denotes the observing time.

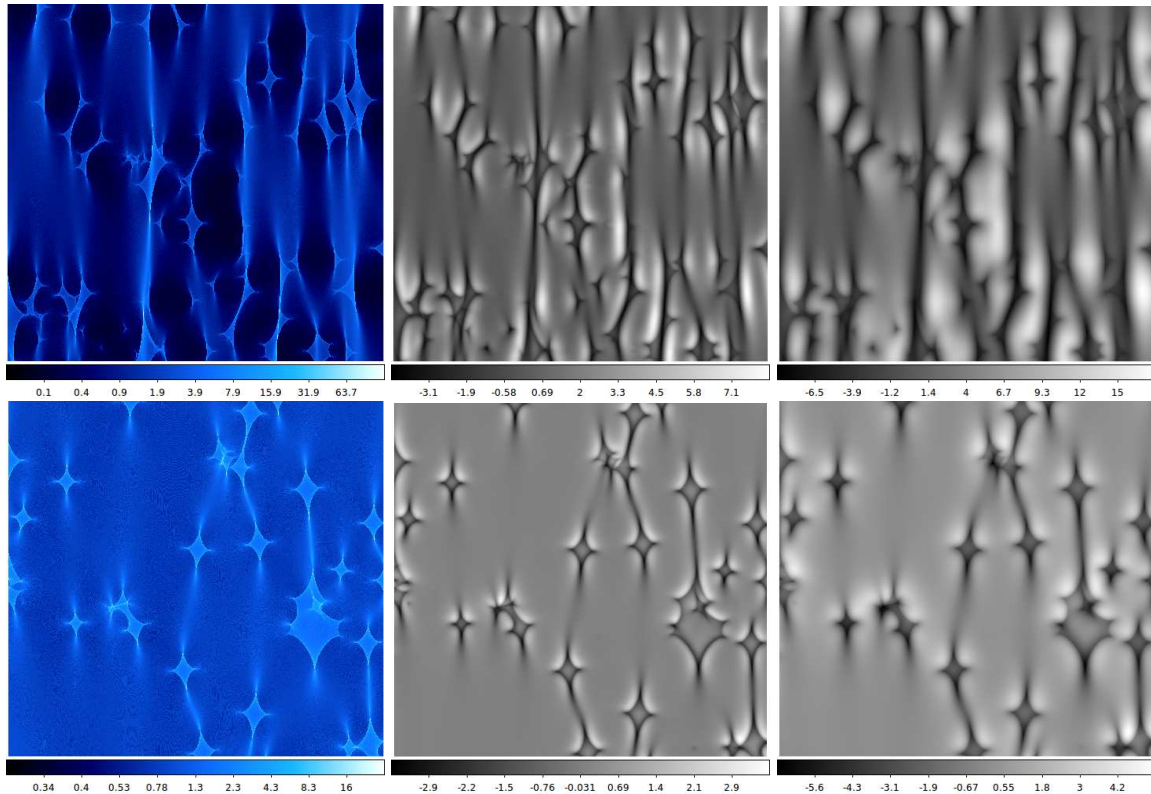


FIG. 1.— Maps for the two images (one of the realizations) in units of day. The blue ones are microlensing magnification maps while the grey ones are microlensing time lag maps. The upper and lower panels are for image B and C, respectively. The middle column corresponds to the standard thin-disk model with disk size R_0 while the left column is for non-standard model with disk size $2R_0$.

3. FINITE LIGHTCURVE CASE

The mean values of the time delay lag maps were found not to be vanished (Tie & Kochanek 2018), suggesting one can not remove such an effect by monitoring the lens for a long period of time. Nevertheless, we conjecture that longer lightcurves may reduce the impact to a level that does not bias H_0 . The disk will cover more parts of the magnification maps with the peculiar motion. Microlensing time delays will therefore slowly change (Tie & Kochanek 2018). Though the changing is hard to be seen since the time scales required must be larger than that typically gives a time delay measurement \sim year(s) (Liao 2020), it actually implies that finite lightcurves could average such an effect.

Microlensing time lags actually depend on observed band and observing epoch $t_{\text{micro}}(b, \mathcal{T})$, so does the measured time delay $\Delta t_{\text{lc}}(b, \mathcal{T})$. The mean value of the measured time delay is

$$\Delta t_{\text{lc}}^{\text{mean}}(b) = \frac{\int \Delta t_{\text{lc}}(b, \mathcal{T}) d\mathcal{T}}{\int d\mathcal{T}}, \quad (8)$$

which is the one reported by the time delay programs like the COSMOGRAIL¹. Note that various algorithms used to give time delay measurements generally work in this way (Liao et. al. 2015): shifting the lightcurves of the lensed images both in flux and time and finding the best-fit values such that the fitness reaches the maximum. During this process, each piece of the light curves are equally considered, i.e., contributing equally. Suppose that each piece gives different time delays, the over-

all best-fit value will be approximately the mean time delay. In the next section, we will conduct a simulation to prove that the dispersion of $\Delta t_{\text{lc}}^{\text{mean}}(b)$ would be smaller than that of $t_{\text{lc}}(b, \mathcal{T})$. Besides, bluer bands like u band with shorter wavelengths will give smaller dispersions than redder bands like r band.

4. SIMULATIONS AND RESULTS

To confirm our conjectures, we do a simulation based on a PG 1115+080-like lensed quasar which has been used in our previous work to deal with the chromatic microlensing time delays (Liao 2020). The redshifts are $z_s = 1.722$ and $z_l = 0.311$ for the source and the lens, respectively. The newest time delay measurements were given by (Bonvin et al. 2018). We take the largest time delay $\Delta t_{\text{lc}}^{\text{BC}} \sim 20$ days between image B and C for example.

The parameters related with microlensing are convergence κ , shear γ and star proportion κ_*/κ . For image B, they are 0.502, 0.811 and 0.331, respectively while for image C, they are 0.356, 0.315 and 0.203, respectively. These values are inferred by macro lens modelling and assuming the stellar mass-luminosity ratio (Chen et al. 2019). We use these parameters to generate microlensing magnification maps for the two images in Fig.1 (the blue ones). The mean stellar mass is set to be $\langle M_* \rangle = 0.3M_\odot$ and the Salpeter mass function is adopted with a ratio of the upper and lower masses being $M_{\text{upper}}/M_{\text{lower}} = 100$. The maps have a size of $20\langle R_{\text{Ein}} \rangle \times 20\langle R_{\text{Ein}} \rangle$ with a pixel resolution of 4096×4096 , where the mean Einstein radius $\langle R_{\text{Ein}} \rangle = 3.6 \times 10^{16}$ cm in the source plane. To avoid the impacts of specific realizations by the random seeds

¹ www.cosmograil.org

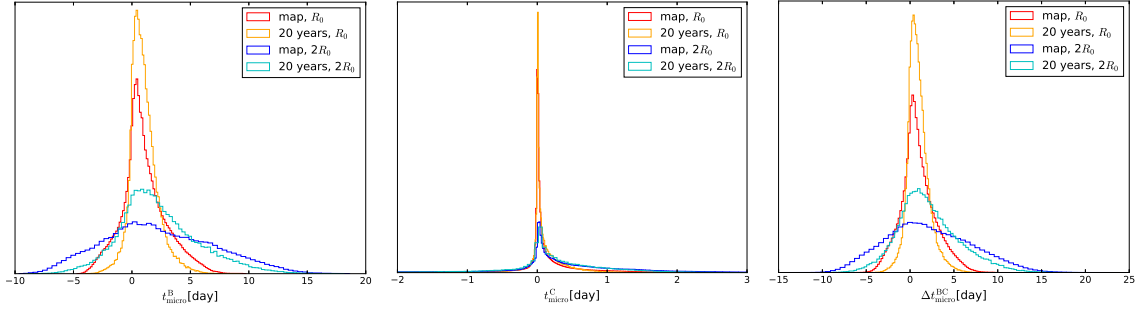


FIG. 2.— Distributions of the mean time lags for the two images (left and middle panels) and mean time delay between them (right panel). Disk sizes R_0 and $2R_0$ are considered, respectively. The red and orange lines termed “map” correspond to the original time lag maps while “20 years” is for finite monitoring.

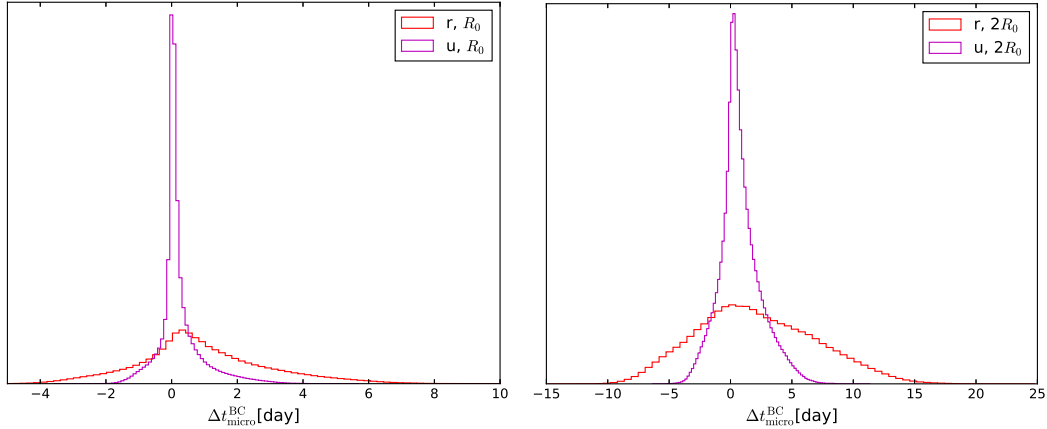


FIG. 3.— Comparisons between r band and u band for disk sizes R_0 and $2R_0$, respectively.

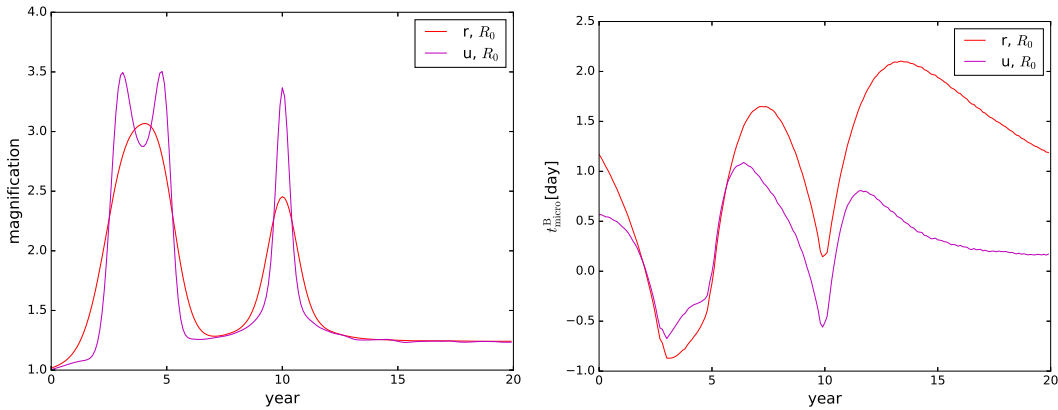


FIG. 4.— An example of image B with disk size R_0 : comparison of microlensing magnification curves between the two bands (left panel) and that of microlensing time lag curves.

used to generate these maps, we actually generate multiple such maps for each image in order to get the average distributions.

Then we calculate the time lag maps using Eq.6. We firstly consider a standard thin-disk model with the disk size R_0 in Eq.1. In addition, we consider a non-standard one which has twice larger disk size $2R_0$. The disk sizes are calculated for u and r bands, respectively: $R_0(r) = 1.63 \times 10^{15}$ cm and $R_0(u) = 7.24 \times 10^{14}$ cm. The central wavelengths are 651nm and 354nm for r band and u band, respectively. Time delay lag map depends on the source configuration, i.e., the inclination angle β and the position angle PA relative to the magnification

map. However, previous studies have found these two parameters impact little on the results. To avoid disorder in the figures and tables, we only consider the case with $\beta = 30^\circ$ and PA=0°. The time lag maps for image B and C in r band are presented in Fig.1 (the grey ones). As one can see, the variations in the maps of image B are much larger than those in image C due to the local environments which generate different magnification maps.

Rather than keeping the source motionless, we consider finite lightcurves corresponding to the trace line of the motion of the source. When calculating the time lag curves or magnification curves, we assume Gaussian dis-

band	campaign	disk size	mean	50th percentile (median)	16th percentile	84th percentile	σ
<i>r</i>	0	R_0	0.915	0.689	-0.844	2.831	1.837
<i>r</i>	20 years	R_0	0.911	0.751	-0.095	1.983	1.039
<i>r</i>	0	$2R_0$	2.110	1.721	-2.793	7.224	5.009
<i>r</i>	20 years	$2R_0$	2.099	1.667	-1.066	5.534	3.300
<i>u</i>	0	R_0	0.215	0.076	-0.155	0.638	0.396
<i>u</i>	0	$2R_0$	0.757	0.528	-0.673	2.328	1.500

TABLE 1

STATISTICS FOR DISTRIBUTIONS IN ALL CASES IN UNITS OF DAY. THE DISPERSION σ IS DEFINED BY PERCENTILE (84TH-16TH)/2.

tributions for the components of the relative velocity v between the source and the star fields in the lens, with standard deviation of 500km/s in each direction. The campaign is considered to be 20 years. For a 500km/s velocity, 20 years' motion corresponds to an angular distance of $\sim 1.5\langle R_{\text{Ein}} \rangle$. We randomly select relative velocities, start points and directions in the maps. Each selection corresponds to a time lag curve and a magnification curve as well for each image. Then we calculate the mean time lags with Eq.3. The distributions of the mean time lags for the two images and the mean time delay between them are shown in Fig.2. Statistics are summarized in Tab.1. As one can see, for a 20-year campaign in r band, the time delay dispersion can be reduced from 1.837 days and 5.009 days to 1.039 days and 3.3 days, for disk sizes R_0 and $2R_0$, respectively. The finite lightcurves reduce the time delay dispersions caused by microlensing typically by $\sim 40\%$.

Moreover, we calculate the microlensing time delay dispersions in u band for disk sizes R_0 and $2R_0$, respectively. The distributions are shown in Fig.3 and the statistics are summarized in Tab.1. The dispersions are reduced by typically $\sim 75\%$. One can easily imagine the case with finite lightcurves in u band (though we do not give the results here) which will be reduced more significantly. While bluer bands give smaller dispersions of microlensing time delays, we want to remind the readers that the microlensing magnification curves would be more undulating and contaminate the shapes of the intrinsic ones more due to the corresponding smaller emission region. To show the anti-relation, we plot Fig.4 where one can see that compared to r band, variation in u band is intenser in the magnification curve and smoother in the microlensing time lag curve. One may doubt that bluer bands always reduce bias. In the TDC, the disk sizes were simulated from 10^{14}cm to 10^{16}cm and no obvious trends were found in the results. Therefore, blue bands like u band will not bias the results from magnification curve aspect. The reason could be the corresponding variation time scales are still larger than the intrinsic ones described by the damped random walk (DRW) pro-

cess.

5. SUMMARY AND DISCUSSIONS

The accuracy of cosmological results becomes more and more important in the current precision cosmology era. Systematic errors and how to control them are worth studying. For strong lens time delay cosmography, one of the systematics comes from the time delay measurements potentially biased by the microlensing time delay effect. In summary, we have proved that increasing the monitoring time and choosing bluer band could indeed reduce the impacts by microlensing on time delay measurements by as large as $\sim 40\%$ and $\sim 75\%$, respectively. Nevertheless, the results show such an effect can not be eliminated and further studies are required to infer an unbiased H_0 , especially for systems like PG 1115+080 having short time delays.

We only discuss the observation strategies for the given lens. In fact, in addition to the band and the campaign length, factors like the redshifts, black hole mass and local environments of the images should be incorporated into the consideration as well. For example, the $\kappa, \gamma, \kappa_*/\kappa$ of image B generates more significant effects than those of image C, suggesting one can find lenses whose all images generate small time lag dispersions and therefore making the time delay measurements nearly unbiased. In the appendix of (Liao et. al. 2015), the standard deviation of magnification map as a function of $\kappa, \gamma, \kappa_*/\kappa$ was studied. Since the time lag map traces magnification map, one can easily find the best point in the parameter space that generates minimum time lag dispersion. Although realistic lens findings and analysis need to consider more factors, our results could be the theoretical guidance.

ACKNOWLEDGMENTS

This work was supported by the National Natural Science Foundation of China (NSFC) No. 11973034 and the Fundamental Research Funds for the Central Universities (WUT: 2020IB022).

REFERENCES

- Birrer S., Amara A., & Refregier A. 2016, JCAP, 8, 020
 Bonvin V., Chan J. H. H., Millon M., et al. 2018, A&A, 616, A183
 Cackett E. M., Horne K., & Winkler H., 2007, MNRAS, 380, 669
 Chen G. C.-F., Chan J. H. H., Bonvin V., et al. 2018, MNRAS, 481, 1115
 Chen G. C.-F., Fassnacht C. D., Suyu S. H., et al. 2019, MNRAS, 490, 1743
 Collier S. J., Horne K., Kaspi S., et al. 1998, ApJ, 500, 162
 Ding X., Treu T., Birrer S., et al. 2020, arXiv: 2006.08619
 Fausnaugh M. M., Denney K. D., Barth A. J., et al. 2016, ApJ, 821, 56
 Jiang Y.-F., Green P. J., Greene J. E., et al. 2017, ApJ, 836, 186
 Liao K., Treu T., Marshall P., et. al. 2015, ApJ, 800, 11
 Liao K. 2020, arXiv: 2007.09379
 MacLeod C. L., Morgan C. W., Mosquera A., et al. 2015, ApJ, 806, 258
 Millon M., Galan A., Courbin F., et al. 2019, arXiv: 1912.08027
 Mosquera A. M., Kochanek C. S., Chen B., et al. 2013, ApJ, 769, 53
 Morgan C. W., Kochanek C. S., Morgan N. D., & Falco E. E. 2010, ApJ, 712, 1129
 Planck Collaboration et al. 2018, arXiv:1807.06209
 Pooley D., Blackburne J. A., Rappaport S., & Schechter P. L. 2007, ApJ, 661, 19

- Riess, A. G., Casertano, S., Yuan, W., Macri, L. M., & Scolnic, D. 2019, *ApJ*, 876, 85
- Schneider P., & Sluse D. 2013, *A&A*, 559, A37
- Sergeev S. G., Doroshenko V. T., Golubinskiy Y. V., Merkulova N. I., & Sergeeva E. A. 2005, *ApJ*, 622, 129
- Shakura N. I., & Sunyaev R. A., 1973, *A&A*, 24, 337
- Shappee B. J., Prieto J. L., Grupe D., et al. 2014, *ApJ*, 788, 48
- Tie S. S., & Kochanek C. S., 2018, *MNRAS*, 473, 80
- Treu T., & Marshall P. J. 2016, *A&ARv*, 24, 11
- Wong K. C., Suyu S. H., Chen G. C.-F., et al. 2020, [arXiv:1907.04869](https://arxiv.org/abs/1907.04869)